Monolithically integrated ultralow threshold topological corner state nanolasers on silicon

Taojie Zhou[1,3,†], Jingwen Ma[2,†], Mingchu Tang[3,†], Haochuan Li[1], Mickael Martin[4], Thierry Baron[4], Huiyun Liu[3,*], Siming Chen[3,*], Xiankai Sun[2,*] and Zhaoyu Zhang[1,5*]

[1] School of Science and Engineering, The Chinese University of Hong Kong, Shenzhen, Guangdong, 518172, P.R. China

[2]Department of Electronic Engineering, The Chinese University of Hong Kong, Shatin, New Territories, Hong Kong

[3]Department of Electronic and Electrical Engineering, University College London, London, WC1E 7JE, United Kingdom

[4]Univ. Grenoble Alpes, CNRS, CEA-LETI, MINATEC, LTM, F-38054 Grenoble, France

[5]Peng Cheng Laboratory

[†]These authors contributed equally to this work

*Corresponding author: huiyun.liu@ucl.ac.uk(H.L.); siming.chen@ucl.ac.uk (S.C.); xksun@cuhk.edu.hk(X.S); zhangzy@cuhk.edu.cn(Z.Z)

ABSTRACT: Monolithic integration of energy-efficient and ultracompact light sources on industry-standard Si platform has emerged as a promising technology to realize fully integrated Si-based photonic integrated circuits. Recently, semiconductor topological lasers by using topologically protected defect modes have received extensive investigations, owing to their unique merits including robustness against structural imperfections and disorders. However, due to the significant material dissimilarities between Si and III–V materials, previous demonstrations of semiconductor topological lasers have been limited on their native substrates. Here, we experimentally report ultralow threshold continuous-wave optically pumped single-mode InAs/GaAs quantum dot topological corner state nanolasers monolithically integrated on CMOS-compatible Si (001) substrate. Our results represent a new route towards ultracompact and high-performance integrated nanoscale light sources for Si photonics and enable promising applications for topological photonics.

KEYWORDS: *Nanolaser, Topological Insulator Laser, Corner State Nanolaser, Silicon Photonics, Quantum Dot*

INTRODUCTION

Topological insulators (TIs) system, originating from condensed-matter physics, has attracted great attentions in photonics and becomes a new strategy to manipulate the behavior of photons at nanoscale[1-3]. Regardless of the specific configurations, most topological photonic systems share a remarkable property named "bulk-boundary correspondence"[4, 5]: *d*-dimensional (*d*D) TIs with their bulk topological order equals to *n* can support (*d*−*n*)-dimensional boundary states at their boundaries. To date, many experiments on topological photonic systems are limited to first-order topological insulators ($n = 1$), for instance quantum Hall, quantum spin Hall, and quantum valley Hall phases[2, 6, 7]. In addition, high-order topological insulators (HOTIs) with $n > 1$ have emerged as an important extension of conventional first-order TIs[8-14]. Along this direction, 2D PhC structures exhibiting second-order topology and supporting 0D topological corner state have aroused broad interests and led to many interesting phenomena[13, 15-17]. Particularly, implementing high-order topological corner state in active media provides a new paradigm in constructing nanolasers with ultracompact footprints, single-mode lasing emission, and most importantly the inherent robustness against perturbations and defects[18-20]. However, room-temperature continuous-wave (CW) nanolasers based on topological corner state have remained experimentally unreported so far with either quantum-well (QW) or quantum dots (QDs) as the gain materials owing to the strict requirements for lasing operation[18-20], harassing their practical applications in on-chip light sources.

In addition, Si-based photonic integrated circuits (PICs) have been regarded as a promising candidate to realize the denser, faster and more energy-efficient chip-scale data communication network[21-25]. Among all the components in Si-based PICs, high-performance lasers on Si remain to be challenging due to the indirect bandgap property of bulk Si[26]. Though topological hybrid integrated III-V/Si microring laser array has been demonstrated by using the direct bonding method[27], topological III-V lasers monolithically integrated on Si is more attractive for large scale, low-cost, and streamlined fabrication[28]. Recently, monolithic integration of III-V lasers on Si platform has fueled impressive developments and many conventional lasers directly grown on Si have been realized,

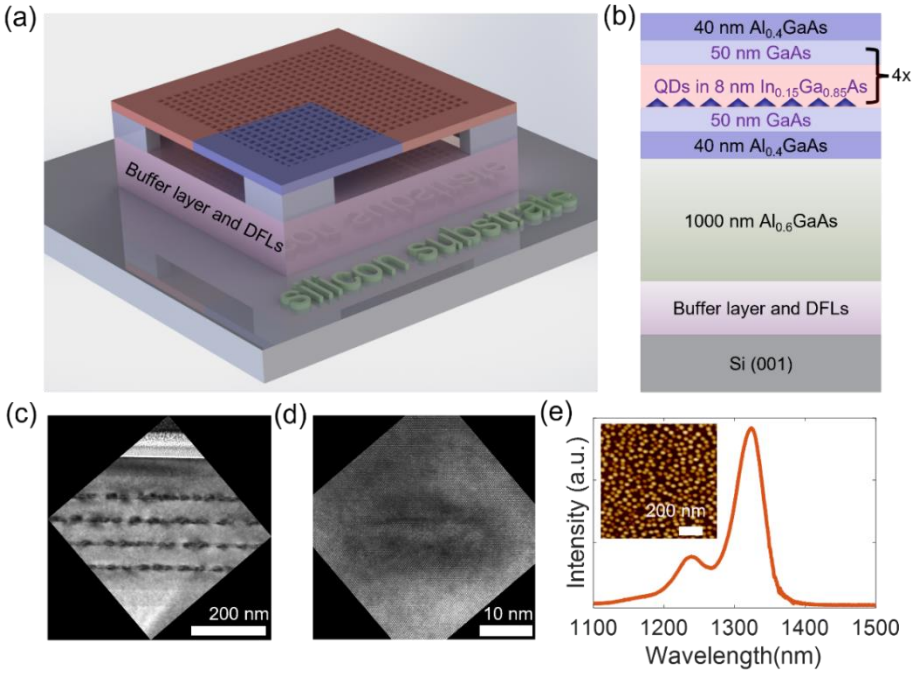

Figure 1. Structure of topological corner state nanolasers on silicon. (a) Schematic structure of the fabricated topological corner state nanolasers monolithically integrated on CMOS-compatible silicon substrate. (b) Schematic illustration of the epitaxial structure. (c), (d) High-resolution TEM images of the four stacked InAs/GaAs QDs and a single QD in the active region, respectively. (e) Measured PL spectra of as-grown InAs/GaAs QDs on silicon. The inset depicts an AFM image of uncapped QDs grown on silicon.

including whispering gallery mode microlasers[29, 30], nano-ridge lasers[31] and PhC lasers[32, 33], while high-order topological nanolasers monolithically grown on Si have remained elusive, which are fundamentally important to construct robust and reliable nanoscale light sources for Si-based PICs.

In this work, we experimentally demonstrate high-order topological PhC nanolasers directly grown on CMOS-compatible Si platform by using InAs/GaAs QDs as the active material. Lasing action at the nanoscale based on the 0D topological corner state was observed with a stable single-mode emission. Mainly owing to the low transparent carrier density, 3D carrier confinement and suppressed thermal effects of as-grown QD gain material, the monolithically integrated InAs/GaAs QD topological nanolasers operated at room temperature with an ultralow lasing threshold around 3 μW under the CW optical pumping conditions. Our results not only indicate great prospects for practical topological PICs with high-performance topological nanolasers, but also provide an important step towards ultracompact light sources monolithically integrated on the Si platform.

EPITAXIAL GROWTH OF QDs ON Si

The InAs/GaAs QD topological corner state nanolasers were monolithically grown on planar on-axis Si (001) substrate. Figure 1a depicts a schematic diagram of the monolithically integrated topological corner state PhC nanolaser on CMOS-compatible silicon substrate. Figure 1b illustrates the epitaxial structure of the grown QD lasers on Si, consisting of four-stack well-developed InAs/$In_{0.15}Ga_{0.85}As$/GaAs dot-in-well (DWELL) active layers. To overcome the antiphase boundaries (APBs) problem, metal-organic chemical vapour deposition was used to grow a two-step 400 nm APB-free epitaxial GaAs film on a pre-treated bi-atomic Si (001) substrate. A 200-nm-thick GaAs buffer layer was grown on the on-axis (001) GaAs/ Si substrate for realizing a smooth surface at 590 °C, followed by growing four sets of defect filter layers (DFLs) to suppress the propagation of threading dislocations[34]. Each set of DFLs included five sets of $In_{0.18}Ga_{0.82}As$/GaAs strained-layer superlattices grown at 480 °C and a 300-nm-thick GaAs spacing layer grown at 590 °C[35]. Then 1-μm-thick $Al_{0.6}Ga_{0.4}As$ sacrificial layer was grown at 600 °C, which was further wet-etched to form a suspending thin PhC slab. Four layers of InAs/$In_{0.15}Ga_{0.85}As$/GaAs DWELL structure between the upper and lower 40-nm-thick $Al_{0.4}Ga_{0.6}As$ cladding layer were grown at the same temperature. Each layer of DWELL structure consisted of three monolayers of InAs QD deposited on a 2-nm-thick $In_{0.15}Ga_{0.85}As$ QW and was capped by a 6 nm $In_{0.15}Ga_{0.85}As$ layer at 510 °C. The DWELL structures were separated by a 50 nm GaAs spacing layer grown at 590 °C[36]. Figures 1c and 1d show high-resolution TEM images of the four stacked InAs/GaAs QDs and a single QD in the active region, respectively. Figure 1e presents the spontaneous emission spectra of as-grown InAs/GaAs QDs on silicon measured at room temperature, which indicates the ground state emission centring at ~ 1.3 μm in O-band with a full width at half maximum of 28 meV. The inset in Figure 1e depicts an atomic force microscope (AFM) image of uncapped InAs/GaAs QDs grown on Si (001) substrate, presenting a good uniformity with a density of ~ 4×10^{10} cm^{-2}.

DEVICE STRUCTURE

Two kinds of topologically distinct square-lattice PhC structures, as indicated by different colours of the PhC regions in Figure 1a, are used to construct the slab-type topological

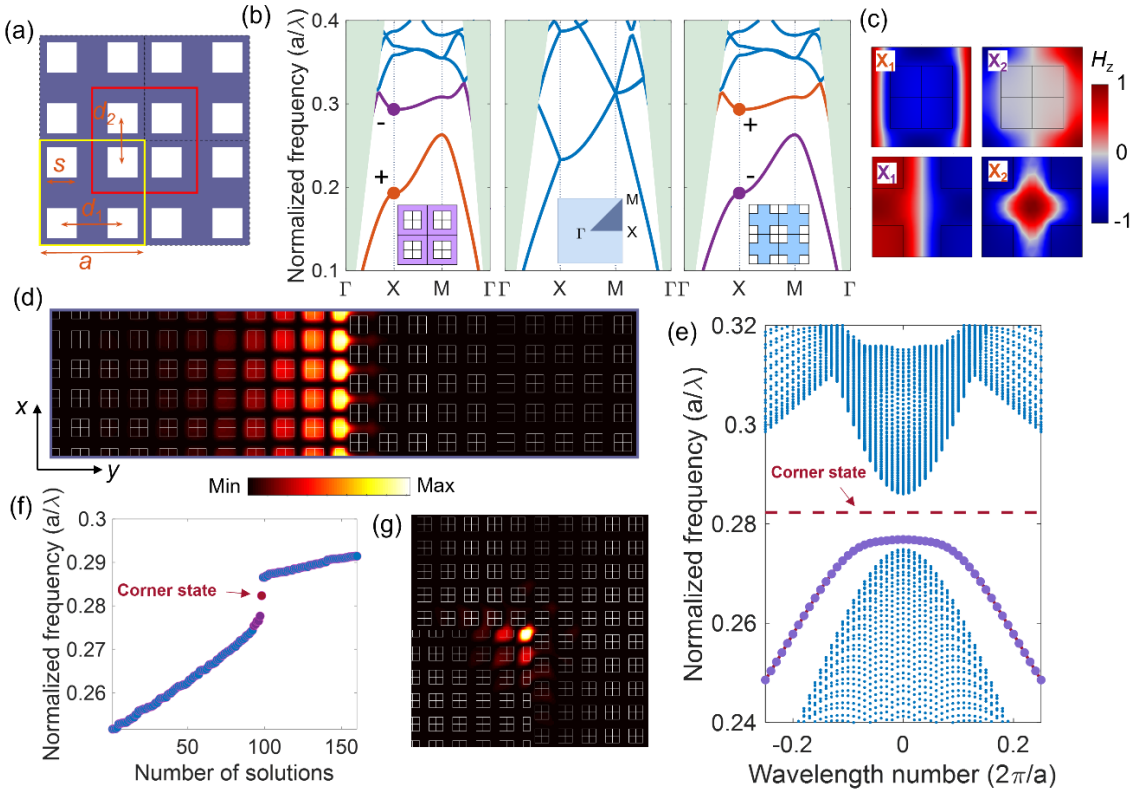

Figure 2. Photonic band diagram and topological states. (a) The unit cell of 2D square-lattice PhC slab with lattice constant a, enclosed by solid yellow line, is consisted of four square-shaped air-holes with side length s and intra- (inter-) separation distance d_1 (d_2). (b) Calculated TE-like photonic band diagram of a 362 nm-thick PhC slab with various δ_d values by assuming a refractive index $n = 3.4$ of the thin slab. From left to right: $\delta_d = d_2 - d_1 = 0.6 * a$ (topologically trivial phase), $\delta_d = 0$, $\delta_d = d_2 - d_1 = -0.6 * a$ (topologically nontrivial phase). The corresponding unit cells (shrunken and expanded structures) are depicted in the inset. + (-) presents the even (odd) parity of the band. (c) Magnetic field (H_z) profiles simulated at the X points for the first (X_1) and second (X_2) energy bands. (d) Calculated magnetic field (H^2) profile at the point $k_x = 0$ for the localized topological 1D edge mode. (e) Calculated projected TE-like photonic band diagram along with the interface. 1D Edge states appear within the first band gap (purple dots). The blue dots correspond to the bulk mode. (f) Calculated photonic eigenmode diagram of the designed topological nanocavity. Edge modes (purple circles) are also marked in the spectrum. (g). Calculated magnetic field (H^2) profile of a topological corner state around the central corner region by using finite-difference time-domain (FDTD) software. The structural parameters for the calculation in (d)-(g): side length $s/a = 0.3$, lattice constant $a = 370$ nm and $n_{eff} = 2.9$.

nanocavity[20]. A topological nontrivial PhC (blue-colored) is surrounded by a trivial PhC region, forming a 90-degree corner along with 1D interfaces. The unit cell of considered 2D square-lattice PhC structure herein is shown in Figure 2a. There are four identical square-shaped air-holes with side length s and intra- (inter-) separation distance d_1 (d_2) within the PhC unit cell. A topological phase transition can be introduced by modifying the intra- (inter-) separation distance. The four sub-squares in the unit cell within the yellow (red) outline are relatively far away from (adjacent to) each other, corresponding to an expanded (shrunken) PhC structure with $\delta_d = d_2 - d_1 < 0$ ($\delta_d = d_2 - d_1 > 0$). The distinct unit cells are coincident with each other when shifting their positions by half a period in both x and y directions. Therefore, the two PhC structures share identical optical band diagram while presenting different topologies as shown in Figure 2b. The TE-like photonic band diagrams with various δ_d values are calculated by using the plane-wave expansion method[37]. The PhC structure with $\delta_d = 0$ exhibits a gapless double degenerate band diagram between X and M points of the first Brillouin zone due to the band folding. For the expanded and shrunken PhC lattices, the degeneracy of the first and second bands at the X point are lifted due to the different parities of their bulk Bloch modes. Figure 2c depicts the magnetic field profile in a unit cell at the X point of the first and second energy bands.

The PhC slab is the photonic realisation of the 2D generalisation of Su-Schrieffer-Heeger (SSH) model[8, 9, 38]. Before studying the high-order topological corner state nanocavity, we first

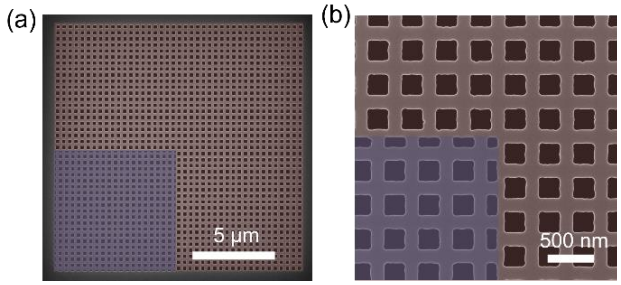

Figure 3. Device fabrication. (a) False-color SEM image of a fabricated device with lattice constant $a = 370$ nm and side length $s/a = 0.3$. (b) A zoomed-in SEM image around the corner region.

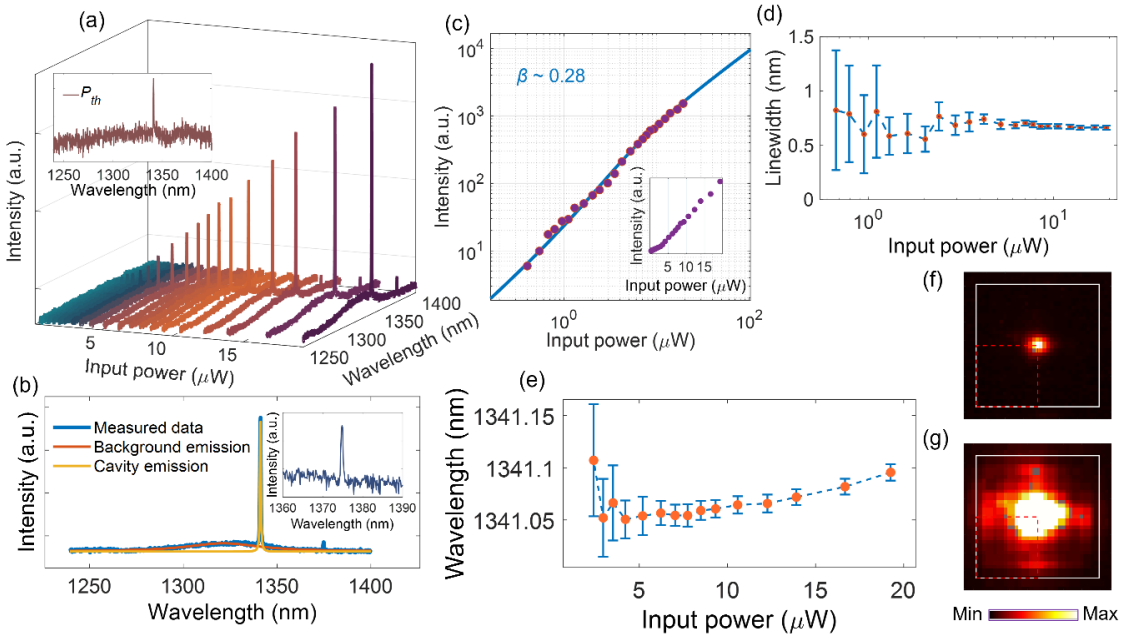

Figure 4. Optical characterisation of topological corner state nanolasers on silicon. (a) Power-dependent lasing spectra of a topological nanolaser on Si. The inset displays a spectrum collected near the threshold. (b) Collected spectra above the threshold and curve fitting showing the spontaneous emission background and cavity emission. The inset depicts an enlarged spectrum indicating an edge mode resonating at longer wavelength compared with corner state. (c) Logarithmic plot of *L-L* curve. The inset presents *L-L* curve in a linear scale. Dots show the experimental data, and the blue line is theoretically calculated result by using rate equation analysis. (d) Linewidth of lasing peak under various input powers. (e) Measured lasing wavelength under various incident powers. (f), (g) The mode pattern measured below and above threshold, respectively.

verified the bulk-edge correspondence and 1D edge state at a straight interface between two topologically distinguished PhC structures. The topologically trivial PhC can suppress the leakage of confined edge modes from the topological nontrivial PhC region. A calculated magnetic field profile for the 1D edge state at point $k_x = 0$ of a straight interface is shown in Figure 2d. The distribution of the magnetic field is strongly localized at the interface, confirmed as 1D edge state propagating along the topological interface. Figure 2e illustrates the projected TE-like photonic band diagram along with the interface calculated by using COMSOL Multiphysics, presenting 1D topological edge state (purple dots) within the bulk bandgap. A dashed line indicating the frequency position of 0D corner state is also plotted in Figure 2e. Then, the 0D topological corner state was numerically investigated. The topological nanocavity is constructed such that the topological nontrivial PhC structure ($\delta_d < 0$) is surrounded by the topological trivial structure ($\delta_d > 0$), forming a 90-degree corner along with 1D interfaces. Figure 2f displays the calculated photonic eigenfrequencies of the topological nanocavity at normalized frequency (a/λ) between 0.25 and 0.3. There is a 0D topological corner state within the photonic band gap, of which the light intensity is tightly localized around the corner region as shown in Figure 2g.

OPTICAL CHARACTERISATION OF TOPOLOGICAL NANOLASERS ON SI

The topological insulator nanolasers based on the topological corner state were fabricated on the CMOS-compatible Si substrate[32]. First, a layer of 120-nm-thick SiO_2 was deposited on the as-grown wafer by plasma-enhanced chemical vapor deposition as hard mask. Then the topological nanocavity pattern was defined by electron-beam lithography and was transferred onto hard mask by plasma etching process. After removing the electron-beam resist, the PhC structures within active slab were formed by using chlorine-based inductively coupled plasma reactive ion etching (ICP-RIE). Finally, wet-etching method was subsequently performed to remove the residual hard mask and the sacrificial layer ($Al_{0.6}Ga_{0.4}As$) to form suspended topological nanocavities. Figure 3a presents a false-color scanning electron microscope (SEM) image of a fabricated topological nanocavity with lattice constant a = 370 nm and side length s/a = 0.3, with 40 periods of unit cells in both x- and y directions. A zoomed-in SEM image around the corner region is presented in Figure 3b, which also reveals some fabrication fluctuations in the shape of unit cells. However, the designed topological nanocavity can exhibit a good robustness to fabrication imperfection, including the disorders in the shape and misalignment of desired photonic crystal pattern.[39] The fabricated topological corner state nanolasers were CW optically pumped at room temperature by using a 632.8 nm He-Ne laser as excitation light under a micro-photoluminescence (μ-PL) system. The pump spot was carefully located at the central corner region of fabricated devices. Due to the fabrication errors, there was a slight difference between the experimental lasing wavelength and the designed 0D corner state resonant value.

Single-mode lasing emission was observed with an ultralow lasing threshold. Figure 4a depicts measured power-dependent spectra of a single-mode topological corner state nanolaser

Table 1. Topological corner state nanolasers.

Ref.	Integrated on silicon	Operation temperature	Gain material	CW	P_{th} (μW)
Ref.18	No	RT	QW	No	5500
Ref.19	No	RT	QW	No	400
Ref.20	No	T = 4.2 K	QD	Yes	1
This work	Yes	RT	QD	Yes	3

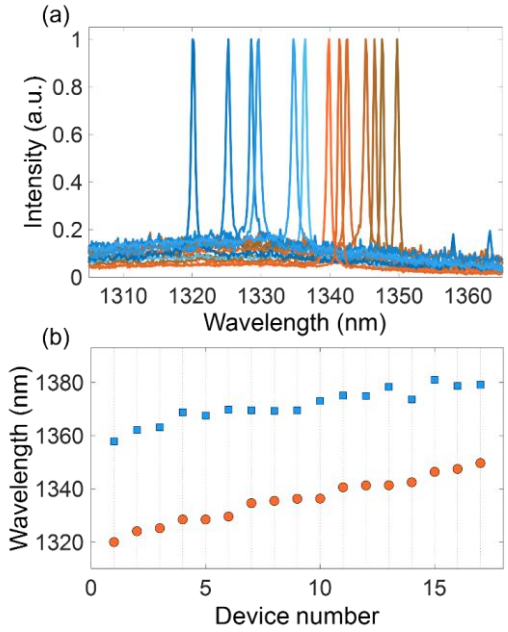

Figure 5. (a) Normalized lasing spectra of several representative topological corner state nanolasers. (b) Positions of corner state modes (yellow circles) and edge state modes (blue squares) of fabricated topological corner state nanolasers on Si. The device number represents various fabricated devices.

with lattice constant a = 370 nm and side length s/a = 0.3. The spectrum shown in the inset of Figure 4a was measured near the threshold. A single sharp resonant peak at 1341 nm grew up from the spontaneous emission background with a transition from spontaneous to stimulated emission as increasing the excitation powers. Figure 4b demonstrates the curve fitting of a spectra measured at 19.3 μW, consisting of a clamped spontaneous emission background and a strong cavity emission. Along with the corner state lasing mode, a topological edge mode resonant peak appears at longer wavelength (1375 nm) under high excitation powers as shown in the inset in Figure 4b, which is mainly caused by the slight overlap of excitation spot at the edge interface region. While the topological edge state is suppressed and fails to reach stimulated emission even under elevated input powers. The logarithmic plot of *L*-*L* (light-out versus light-in) curve (shown in Figure 4c) presents a soft turn-on of the laser operation with a mild "*s*" shape, indicating a typical behavior of nanolaser with high spontaneous emission coupling factor (β). The β factor, evaluated approximately 0.28, is extracted by fitting the experimental data with semiconductor rate equation model [32]. A clear kink is observed in the *L*-*L* curve on a linear scale (see inset in Figure 4c). The lasing threshold (P_{th}) is estimated at ~ 3 μW from the *L*-*L* curve, which is comparable to previously demonstrated *L*3 defect PhC nanolasers with the same epitaxial structure[32]. Particularly, as summarized in Table 1, the fabricated QD topological nanolaser has a much lower threshold compared with reported QWs-based topological corner state nanolasers. Both the remarkable low transparent carrier density according to the δ-function-like density of states and 3D carrier confinement in a QD system[40], which are among the most important characteristics of QD lasers, play significant roles in reducing the detrimental thermal effects and enabling the CW laser operation at room temperature with much lower threshold compared with topological QW nanolasers. The high crystal quality, high β factor, and reduced nonradiative recombination rate also contribute to the low threshold and CW laser operation. In addition, the low threshold operation of integrated QD topological corner state nanolasers on Si was compatible to their topologically trivial counterparts on its native substrate[40, 41]. As shown in Figure 4d, the linewidth narrowing effect with a narrow linewidth (~ 0.66 nm) above threshold is observed, which verifies the lasing emission. The cavity quality factor is approximately estimated from the linewidth just below the threshold, where the optical loss by the absorption of QDs is very weak. The linewidth measured at just below the threshold corresponds to a value of quality factor ~ 1960, which is much smaller than the theoretical value of 10300 mainly due to the structural imperfection and roughness. Figure 4e displays a red shift of the measured lasing wavelengths with increasing incident powers mainly induced by thermal effects. To further examine the lasing mode, the mode pattern was taken by an infrared camera as depicted in Figure 4f and Figure 4g. The mode patterns collected below and above the threshold presented a strong light spot localized at the central cavity region, which confirmed the lasing emission from topological corner state. The lasing wavelengths were finely tuned by varying the side length s/a from 0.27 to 0.32 while keeping the lattice constant a = 370 nm of designed topological nanolaser array, as illustrated in Figure 5a. Among fabricated nanolasers, edge state resonant modes existed at longer wavelength under elevated excitation powers. The peak positions of corner state lasing mode and resonant mode at edge state are depicted in Figure 5b. The experimental free spectra range between the corner state and the edge state mode was consistent with the simulated values.

CONCLUSION

In conclusion, we demonstrate QD topological corner state nanolasers monolithically integrated on CMOS-compatible Si platform. Stable single-mode lasing emission with an ultralow threshold ~ 3 μW and a high spontaneous emission coupling factor estimated at ~ 0.28 were achieved at room temperature under CW optical pumping conditions. More recently, we presented topological vertical emission Dirac-vortex microscale lasers monolithically integrated on silicon[42], while the topological nanolasers demonstrated here exhibit a much smaller mode volume and a lower lasing threshold. Our results not only indicate great potential for manipulating the generation of light at nanoscale in topological nanophotonic circuits, but also provide an important step towards ultracompact high-performance light sources monolithically integration on the silicon platform.

AUTHOR CONTRIBUTION

T.Z. and J.M. fabricated the devices. M.T., M.M., and T.B. epitaxially grew the III–V-on-silicon materials. T.Z. conducted the optical characterisation and the numerical simulation. T.Z. wrote the manuscript with input from all authors. All the authors contributed to the manuscript. H.L., S.C., X.S. and Z.Z. supervised the project.

Notes The authors declare no conflict of interest.

FUNDING

The research grants Shenzhen Key Laboratory Project (ZDSYS201603311644527), Optical Communication Core Chip Research Platform, National Natural Science Foundation of China (62174144), Shenzhen Fundamental Research Fund (JCYJ20210324115605016, JCYJ20210324120204011), The Major Key Project of PCL(PCL2021A14), Council of Hong Kong (14209519), UK Engineering and Physical Sciences Research Council (EP/P006973/1, EP/T01394X/1, EP/T028475/1), National Epitaxy Facility, European project H2020-ICT-PICTURE (780930), Royal Academy of Engineering (RF201617/16/28), French National Research Agency under the Investissements d'avenir ANR-10-IRT-05 and ANR-15-IDEX-02 and French RENATECH network.

REFERENCES

(1) Bandres, M. A.; Wittek, S.; Harari, G.; Parto, M.; Ren, J.; Segev, M.; Christodoulides, D. N.; Khajavikhan, M., Topological insulator laser: Experiments. *Science* **2018,** *359* (6381), eaar4005.
(2) Barik, S.; Karasahin, A.; Flower, C.; Cai, T.; Miyake, H.; DeGottardi, W.; Hafezi, M.; Waks, E., A topological quantum optics interface. *Science* **2018,** *359* (6376), 666-668.
(3) Choi, J.-H.; Hayenga, W. E.; Liu, Y. G.; Parto, M.; Bahari, B.; Christodoulides, D. N.; Khajavikhan, M., Room temperature electrically pumped topological insulator lasers. *Nat. Commun.* **2021,** *12* (1), 1-7.
(4) Schindler, F.; Cook, A. M.; Vergniory, M. G.; Wang, Z.; Parkin, S. S. P.; Bernevig, B. A.; Neupert, T., Higher-order topological insulators. *Sci. Adv.* **2018,** *4* (6), eaat0346.
(5) Benalcazar, W. A.; Bernevig, B. A.; Hughes, T. L., Quantized electric multipole insulators. *Science* **2017,** *357* (6346), 61-66.
(6) Zeng, Y.; Chattopadhyay, U.; Zhu, B.; Qiang, B.; Li, J.; Jin, Y.; Li, L.; Davies, A. G.; Linfield, E. H.; Zhang, B.; Chong, Y.; Wang, Q. J., Electrically pumped topological laser with valley edge modes. *Nature* **2020,** *578* (7794), 246-250.
(7) Ma, J.; Xi, X.; Li, Y.; Sun, X., Nanomechanical topological insulators with an auxiliary orbital degree of freedom. *Nat. Nanotechnol* **2021,** *16* (5), 576-583.
(8) Liu, F.; Wakabayashi, K., Novel Topological Phase with a Zero Berry Curvature. *Phys. Rev. Lett.* **2017,** *118* (7), 076803.
(9) Xie, B.-Y.; Wang, H.-F.; Wang, H.-X.; Zhu, X.-Y.; Jiang, J.-H.; Lu, M.-H.; Chen, Y.-F., Second-order photonic topological insulator with corner states. *Phys. Rev. B* **2018,** *98* (20), 205147.
(10) Ota, Y.; Liu, F.; Katsumi, R.; Watanabe, K.; Wakabayashi, K.; Arakawa, Y.; Iwamoto, S., Photonic crystal nanocavity based on a topological corner state. *Optica* **2019,** *6* (6), 786-789.
(11) Xie, B.; Wang, H.-X.; Zhang, X.; Zhan, P.; Jiang, J.-H.; Lu, M.; Chen, Y., Higher-order band topology. *Nat. Rev. Phys.* **2021**, 1-13.
(12) Schindler, F.; Cook, A. M.; Vergniory, M. G.; Wang, Z.; Parkin, S. S.; Bernevig, B. A.; Neupert, T., Higher-order topological insulators. *Sci. Adv.* **2018,** *4* (6), eaat0346.
(13) Kruk, S. S.; Gao, W.; Choi, D.-Y.; Zentgraf, T.; Zhang, S.; Kivshar, Y., Nonlinear Imaging of Nanoscale Topological Corner States. *Nano Lett.* **2021,** *21* (11), 4592-4597.
(14) He, X.-T.; Li, M.-Y.; Qiu, H.-Y.; Ruan, W.-S.; Zhou, L.-D.; Liu, L.; Chen, X.-D.; Chen, W.-J.; Zhao, F.-L.; Dong, J.-W., In-plane excitation of a topological nanophotonic corner state at telecom wavelengths in a cross-coupled cavity. *Photon. Res.* **2021,** *9* (8), 1423-1431.
(15) Li, M.; Zhirihin, D.; Gorlach, M.; Ni, X.; Filonov, D.; Slobozhanyuk, A.; Alù, A.; Khanikaev, A. B., Higher-order topological states in photonic kagome crystals with long-range interactions. *Nat. Photonics* **2019,** *14* (2), 89-94.
(16) Xie, X.; Zhang, W.; He, X.; Wu, S.; Dang, J.; Peng, K.; Song, F.; Yang, L.; Ni, H.; Niu, Z., Cavity Quantum Electrodynamics with Second-Order Topological Corner State. *Laser Photonics Rev.* **2020,** *14* (8), 1900425.
(17) Xie, B. Y.; Su, G. X.; Wang, H. F.; Su, H.; Shen, X. P.; Zhan, P.; Lu, M. H.; Wang, Z. L.; Chen, Y. F., Visualization of Higher-Order Topological Insulating Phases in Two-Dimensional Dielectric Photonic Crystals. *Phys. Rev. Lett.* **2019,** *122* (23), 233903.
(18) Han, C.; Kang, M.; Jeon, H., Lasing at Multidimensional Topological States in a Two-Dimensional Photonic Crystal Structure. *ACS Photonics* **2020,** *7* (8), 2027-2036.
(19) Kim, H. R.; Hwang, M. S.; Smirnova, D.; Jeong, K. Y.; Kivshar, Y.; Park, H. G., Multipolar lasing modes from topological corner states. *Nat. Commun.* **2020,** *11* (1), 5758.
(20) Zhang, W.; Xie, X.; Hao, H.; Dang, J.; Xiao, S.; Shi, S.; Ni, H.; Niu, Z.; Wang, C.; Jin, K.; Zhang, X.; Xu, X., Low-threshold topological nanolasers based on the second-order corner state. *Light: Sci. Appl.* **2020,** *9*, 109.
(21) Sun, C.; Wade, M. T.; Lee, Y.; Orcutt, J. S.; Alloatti, L.; Georgas, M. S.; Waterman, A. S.; Shainline, J. M.; Avizienis, R. R.; Lin, S., Single-chip microprocessor that communicates directly using light. *Nature* **2015,** *528* (7583), 534-538.
(22) Komljenovic, T.; Huang, D.; Pintus, P.; Tran, M. A.; Davenport, M. L.; Bowers, J. E., Photonic integrated circuits using heterogeneous integration on silicon. *Proc. IEEE* **2018,** *106* (12), 2246-2257.
(23) Helkey, R.; Saleh, A. A.; Buckwalter, J.; Bowers, J. E., High-performance photonic integrated circuits on silicon. *IEEE J. Sel. Top. Quantum Electron.* **2019,** *25* (5), 1-15.
(24) Norman, J. C.; Jung, D.; Wan, Y.; Bowers, J. E., Perspective: The future of quantum dot photonic integrated circuits. *APL Photonics* **2018,** *3* (3), 030901.
(25) Soref, R., The past, present, and future of silicon photonics. *IEEE J. Sel. Top. Quantum Electron.* **2006,** *12* (6), 1678-1687.
(26) Liang, D.; Bowers, J. E., Recent progress in lasers on silicon. *Nat. Photonics* **2010,** *4* (8), 511-517.
(27) Zhao, H.; Miao, P.; Teimourpour, M. H.; Malzard, S.; El-Ganainy, R.; Schomerus, H.; Feng, L., Topological hybrid silicon microlasers. *Nat. Commun.* **2018,** *9* (1), 981.
(28) Chen, S.; Li, W.; Wu, J.; Jiang, Q.; Tang, M.; Shutts, S.; Elliott, S. N.; Sobiesierski, A.; Seeds, A. J.; Ross, I., Electrically pumped continuous-wave III–V quantum dot lasers on silicon. *Nat. Photonics* **2016,** *10* (5), 307-311.
(29) Zhou, T.; Tang, M.; Xiang, G.; Fang, X.; Liu, X.; Xiang, B.; Hark, S.; Martin, M.; Touraton, M.-L.; Baron, T.; Lu, Y.; Chen, S.; Liu, H.; Zhang, Z., Ultra-low threshold InAs/GaAs quantum dot microdisk lasers on planar on-axis Si (001) substrates. *Optica* **2019,** *6* (4), 430-435.
(30) Wan, Y.; Li, Q.; Liu, A. Y.; Gossard, A. C.; Bowers, J. E.; Hu, E. L.; Lau, K. M., Optically pumped 1.3 μm room-temperature InAs quantum-dot micro-disk lasers directly grown on (001) silicon. *Opt. Lett.* **2016,** *41* (7), 1664-1667.

(31) Han, Y.; Yan, Z.; Ng, W. K.; Xue, Y.; Wong, K. S.; Lau, K. M., Bufferless 1.5 μm III-V lasers grown on Si-photonics 220 nm silicon-on-insulator platforms. *Optica* **2020,** *7* (2), 148-153.
(32) Zhou, T.; Tang, M.; Xiang, G.; Xiang, B.; Hark, S.; Martin, M.; Baron, T.; Pan, S.; Park, J.-S.; Liu, Z.; Chen, S.; Zhang, Z.; Liu, H., Continuous-wave quantum dot photonic crystal lasers grown on on-axis Si (001). *Nat. Commun.* **2020,** *11* (1), 977.
(33) Zhou, T.; Tang, M.; Li, H.; Zhang, Z.; Cui, Y.; Park, J. S.; Martin, M.; Baron, T.; Chen, S.; Liu, H.; Zhang, Z., Single-Mode Photonic Crystal Nanobeam Lasers Monolithically Grown on Si for Dense Integration. *IEEE J. Sel. Top. Quantum Electron.* **2022,** *28* (3), 1-6.
(34) Alcotte, R.; Martin, M.; Moeyaert, J.; Cipro, R.; David, S.; Bassani, F.; Ducroquet, F.; Bogumilowicz, Y.; Sanchez, E.; Ye, Z.; Bao, X. Y.; Pin, J. B.; Baron, T., Epitaxial growth of antiphase boundary free GaAs layer on 300 mm Si(001) substrate by metalorganic chemical vapour deposition with high mobility. *APL Materials* **2016,** *4* (4), 046101.
(35) Tang, M.; Chen, S.; Wu, J.; Jiang, Q.; Kennedy, K.; Jurczak, P.; Liao, M.; Beanland, R.; Seeds, A.; Liu, H., Optimizations of Defect Filter Layers for 1.3-μm InAs/GaAs Quantum-Dot Lasers Monolithically Grown on Si Substrates. *IEEE J. Sel. Top. Quantum Electron.* **2016,** *22* (6), 50-56.
(36) Liu, H. Y.; Sellers, I. R.; Badcock, T. J.; Mowbray, D. J.; Skolnick, M. S.; Groom, K. M.; Gutiérrez, M.; Hopkinson, M.; Ng, J. S.; David, J. P. R.; Beanland, R., Improved performance of 1.3μm multilayer InAs quantum-dot lasers using a high-growth-temperature GaAs spacer layer. *Appl. Phys. Lett.* **2004,** *85* (5), 704-706.
(37) Johnson, S. G.; Joannopoulos, J. D., Block-iterative frequency-domain methods for Maxwell's equations in a planewave basis. *Opt. Express* **2001,** *8* (3), 173-190.
(38) Obana, D.; Liu, F.; Wakabayashi, K., Topological edge states in the Su-Schrieffer-Heeger model. *Phys. Rev. B* **2019,** *100* (7), 075437.
(39) Liu, C.; Maier, S. A., High-Quality Optical Hotspots with Topology-Protected Robustness. *ACS Photonics* **2022,** *9* (1), 241-248.
(40) Nomura, M.; Iwamoto, S.; Watanabe, K.; Kumagai, N.; Nakata, Y.; Ishida, S.; Arakawa, Y., Room temperature continuous-wave lasing in photonic crystal nanocavity. *Opt. Express* **2006,** *14* (13), 6308-6315.
(41) Gong, Y.; Ellis, B.; Shambat, G.; Sarmiento, T.; Harris, J. S.; Vučković, J., Nanobeam photonic crystal cavity quantum dot laser. *Opt. Express* **2010,** *18* (9), 8781-8789.
(42) Ma, J.; Zhou, T.; Tang, M.; Li, H.; Zhang, Z.; Xi, X.; Martin, M.; Baron, T.; Liu, H.; Zhang, Z., Room-temperature continuous-wave Dirac-vortex topological lasers on silicon. *arXiv*, **2021**, https://arxiv.org/abs/2106.13838 (accessed 2021-06-25)

For Table of Contents Use Only

Monolithically integrated ultralow threshold topological corner state nanolasers on silicon

Taojie Zhou[1,3,†], Jingwen Ma[2,†], Mingchu Tang[3,†], Haochuan Li[1], Mickael Martin[4], Thierry Baron[4], Huiyun Liu[3,*], Siming Chen[3,*], Xiankai Sun[2,*] and Zhaoyu Zhang[1,5*]

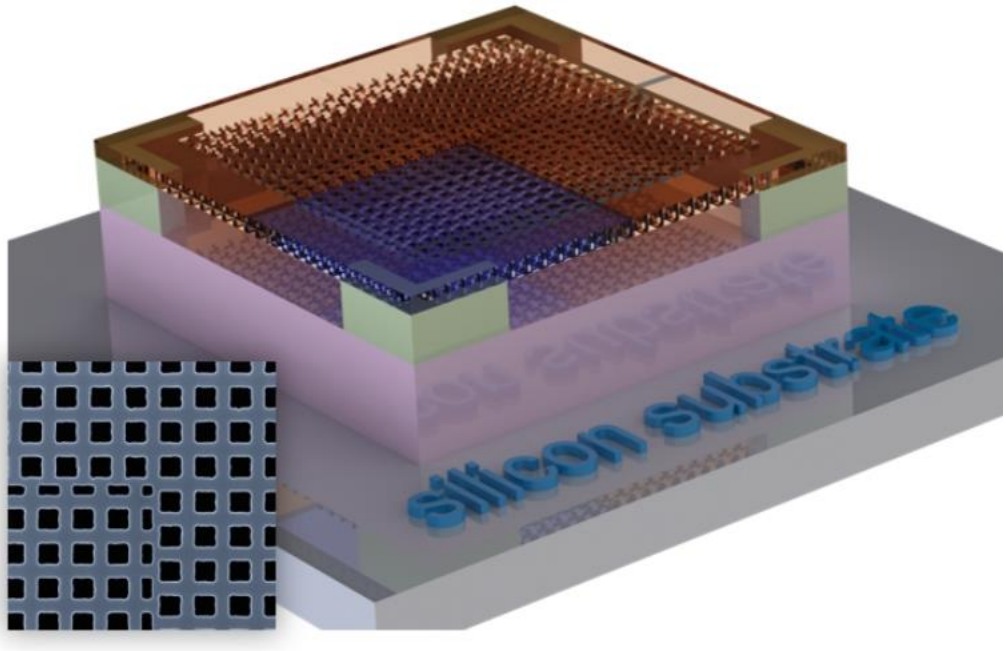

The graphic presents a schematic diagram of topological corner state nanolaser grown on silicon, with a SEM image of fabricated device in the lower left corner.